Quantitative Proteomics Reveals That Hsp90 Inhibition Preferentially Targets Kinases and the DNA Damage Response*[S]

Kirti Sharma‡§, R. Martin Vabulas§¶‖, Boris Macek‡§, Stefan Pinkert¶, Jürgen Cox‡, Matthias Mann‡ ‡‡, and F. Ulrich Hartl¶§§**

Despite the increasing importance of heat shock protein 90 (Hsp90) inhibitors as chemotherapeutic agents in diseases such as cancer, their global effects on the proteome remain largely unknown. Here we use high resolution, quantitative mass spectrometry to map protein expression changes associated with the application of the Hsp90 inhibitor, 17-(dimethylaminoethylamino)-17-demethoxygeldanamycin (17-DMAG). In depth data obtained from five replicate SILAC experiments enabled accurate quantification of about 6,000 proteins in HeLa cells. As expected, we observed activation of a heat shock response with induced expression of molecular chaperones, which refold misfolded proteins, and proteases, which degrade irreparably damaged polypeptides. Despite the broad range of known Hsp90 substrates, bioinformatics analysis revealed that particular protein classes were preferentially affected. These prominently included proteins involved in the DNA damage response, as well as protein kinases and especially tyrosine kinases. We followed up on this observation with a quantitative phosphoproteomic analysis of about 4,000 sites, which revealed that Hsp90 inhibition leads to much more down- than up-regulation of the phosphoproteome (34% down *versus* 6% up). This study defines the cellular response to Hsp90 inhibition at the proteome level and sheds light on the mechanisms by which it can be used to target cancer cells. ***Molecular & Cellular Proteomics 11: 10.1074/mcp.M111.014654, 1–12, 2012.***

All cells invest in a complex machinery of molecular chaperones, heat shock proteins and other factors, to ensure efficient protein folding and the maintenance of the conformational integrity of the proteome (proteostasis) (1). A major role of this machinery is to prevent the accumulation of potentially toxic misfolded or aggregated proteins that are associated with numerous diseases, including type II diabetes, Alzheimer disease, Parkinson disease, Huntington disease, and amyotrophic lateral sclerosis (reviewed in Refs. 2–5). A common cellular reaction to protein misfolding and aggregation brought on by a variety of environmental stressors, such as heat shock, oxidative, or chemical insult, is the up-regulation of heat shock proteins (Hsps)[1] and chaperones. Cancer cells, which depend for uncontrolled growth on a variety of mutated and thus conformationally destabilized signaling proteins, are generally thought to require a higher level of chaperones than nontransformed cells (6). Heat shock protein 90 (Hsp90), an abundant molecular chaperone, participates in these processes in two distinct ways (7). On the one hand, Hsp90 mediates the folding and conformational regulation of numerous signaling proteins, such as proto-oncogenic kinases and steroid receptors. Its inhibition leaves these proteins in an unfolded or partially folded state, exposed to proteasomal degradation. Consequently, Hsp90 inhibition by benzoquinones, such as geldanamycin and derivatives, is explored as a strategy in the therapy of certain cancers (8, 9). On the other hand, Hsp90 plays a key role in the regulation of HSF1, the master transcription factor of the cytosolic stress response. Hsp90 is known to associate with HSF1 and stabilize it in an inactive state (10). Hsp90 inhibitors disrupt this association. Free HSF1 then trimerizes and moves into the nucleus, where it transcriptionally activates the stress response (8, 10, 11). In doing so, geldanamycin can inhibit the aggregation of neurodegenerative disease proteins, such as huntingtin (12).

Because of its importance for normal cellular function and disease, we set out to systematically analyze the consequences of Hsp90 inhibition at the proteome level in human cells. Specifically, we used the Hsp90 inhibitor 17-dimethylaminoethylo-17-demethoxygeldanamycin (17-DMAG), a derivative of geldanamycin with higher potency, better solubility, and less toxicity than geldanamycin (13). 17-DMAG and sim-

From the Departments of ‡Proteomics and Signal Transduction and ¶Cellular Biochemistry, Max-Planck-Institute of Biochemistry, Am Klopferspitz 18, 82152 Martinsried, Germany

⌘ *Author's Choice*—Final version full access.

Received September 24, 2011, and in revised form, November 14, 2011

Published, MCP Papers in Press, December 13, 2011, DOI 10.1074/mcp.M111.014654

[1] The abbreviations used are: Hsp, heat shock protein; 17-DMAG, 17-(dimethylaminoethylamino)-17-demethoxygeldanamycin; SILAC, stable isotope labeling by amino acids in cell culture; HCD, higher energy collisional dissociation; MS/MS, tandem mass spectrometry; GO, Gene Ontology; KEGG, Kyoto Encyclopedia of Gene and Genomes.

ilar inhibitors currently under clinical evaluation interact with the ATP-binding pocket in the N-terminal domain of Hsp90 and disrupt the chaperone cycle, resulting in HSF1 activation and in degradation of Hsp90 substrate proteins via the ubiquitin-proteasome pathway (14–16). The rationale for pursuing the molecular chaperone Hsp90 as a therapeutic target is that its inhibition simultaneously affects multiple client proteins leading to a combinatorial effect on multiple signaling pathways and, consequently, in broad dampening of deregulated cancer signaling (9, 15, 17).

In recent years, accurate quantitative proteomics has evolved into a powerful technology allowing mechanisms of drug actions to be elucidated directly at the proteome level in a system-wide manner (18, 19). Proteome studies have an advantage over transcriptome studies, because by their nature they take post-transcriptional events into account. This is a particular advantage when altered protein degradation is expected to be an important mechanism, as is the case with Hsp90 inhibition. MS-based approaches to the mechanism of drug action can either identify the direct drug-binding targets (20, 21) or identify more downstream signaling molecules by global detection of inhibitor-induced (phospho)proteomic changes in cells (see, for example, Ref. 22). There are several reports of the Hsp90 interactome (23, 24); however, few proteomics studies have investigated the effects of Hsp90 inhibition. Proteomic changes in response to geldanamycin or its analog 17-allylamino-17-demethoxygeldanamycin were monitored by two-dimensional gel electrophoresis or by cleavable isotope-coded affinity tag-based quantitative mass spectrometry (25, 26). The proteome coverage of those studies was limited to the more abundant cellular functions, and the observed changes were diverse and included induction of proteins involved in the 26 S proteasome, signal transduction, protein synthesis and degradation, RNA processing, transcription, cell cycle, and apoptosis.

Here, we combined the SILAC technology (27) and high resolution MS to study system-wide effects of 17-DMAG treatment and the induced heat shock response in HeLa cells at the protein and phosphorylation site levels. From five biological replicates we obtained highly accurate quantifications of an in depth proteome. The aim of our study was to determine—in an unbiased manner—the major functional categories of proteins that are affected by Hsp90 inhibition. To this end, we combined the strength of high accuracy data with a sophisticated bioinformatics algorithm and found that Hsp90 inhibition leads to a tailored cellular response. Our study demonstrates that inhibition of a single chaperone system can have far-reaching effects on numerous key cellular functions. It provides a resource for further studies on the effect of Hsp90 inhibitors.

EXPERIMENTAL PROCEDURES

Cell Culture and Lysate Preparation—Quantitative analysis was based on SILAC (27), which involved HeLa cells grown in Dulbecco's modified Eagle's medium containing either unlabeled L-arginine (Arg^0) and L-lysine or heavy isotope-labeled $^{13}C_6{}^{14}N_4$-L-arginine (Arg^6) and 4,4,5,6-D_4-L-lysine (Lys^4) (Cambridge Isotope Laboratories, Inc.) supplemented with 10% dialyzed fetal bovine serum (Invitrogen). Light labeled cells were left untreated to serve as control and heavy labeled cells were treated with 50 μM of 17-DMAG (Biomol) for 24 h. The cells were washed three times with PBS and lysed in a buffer containing 4% SDS and 0.1 M DTT in 100 mM Tris/HCl, pH 7.6. After 3 min of heating at 95 °C and sonication, the samples were clarified by centrifugation for 10 min at 20,000 $\times$ *g*. Protein content was determined using the BCA protein assay kit (Thermo Fisher Scientific, Rockford, IL) according to the manufacturer's instructions. The experiment was independently performed five times (biological replicates). All of the samples were stored at −80 °C until further parallel processing.

Protein Digestion and Peptide Fractionation—Equal amounts of protein from control and 17-DMAG-treated cells were mixed and further processed for digestion by the filter-aided sample preparation method (28). Briefly, the lysate solubilized in SDS-containing buffer was loaded onto Microcon YM-30 devices (Millipore, Billerica, MA), and SDS from the samples was removed by urea exchange followed by alkylation with 50 mM iodoacetamide. Urea was then replaced with 20 mM ammonium bicarbonate before the proteins were digested overnight at 37 °C with trypsin (Promega) (1 μg of trypsin:100 μg of protein). The peptides were collected from the filter by centrifugation followed by an additional elution with water.

From each biological replicate 70 μg of peptide mixture was separated into six fractions via strong anion exchange chromatography as described (29). Briefly, peptides were loaded into tip columns prepared from 200-μl micropipette tips stacked with six layers of a 3 M Empore anion exchange disk (1214–5012 Varian, Palo Alto, CA). We used Britton & Robinson universal buffer composed of 20 mM acetic acid, 20 mM phosphoric acid, and 20 mM boric acid and titrated with NaOH to the desired pH for column equilibration and elution of fractions. The peptides were loaded at pH 11, and fractions were subsequently eluted with buffer solutions of pH 8, 6, 5, 4, and 3. The eluted peptide fractions were loaded on reversed phase C_{18} StageTips (30). The peptides were eluted twice with 20 μl of buffer B containing 80% ACN in 0.5% acetic acid, and organic solvents were removed in a SpeedVac concentrator before analyzing the eluted peptide mixture by LC-MS.

Sequential Enrichment of Phosphopeptides Using TiO_2 Beads—For phosphopeptide enrichment, the eluted peptides (1 mg) were acidified with trifluoroacetic acid to pH 2.7, and ACN was added to a final concentration of 30%. After measuring their UV absorbance, the peptide samples were incubated with TiO_2 beads (31) (MZ-Analysentechnik) in peptide to bead ratios of either 1:4 or 4:1 (32). For consecutive incubations, the peptide bead slurry was incubated for 30 min and centrifuged, and the supernatant was incubated with another aliquot of freshly prepared TiO_2 beads for the next enrichment. To prevent nonspecific binding, the TiO_2 beads were resuspended in a 30 mg/ml solution of dihydrobenzoic acid (Sigma) prepared in 75% ACN and 0.1% TFA (33). After incubating with the peptide mix, the beads were washed with 30% ACN and 3% TFA twice followed by two washes with 75% ACN and 0.3% TFA. The phosphopeptides were then eluted using elution buffer containing 15% ammonium hydroxide and 40% ACN. Finally, the eluted phosphopeptides were loaded on C_{18} StageTips. For LC-MS/MS analysis, the phosphopeptides were eluted as described above for peptides except that the elution buffer was comprised of 60% ACN in 0.5% acetic acid (34).

Mass Spectrometry—Peptide mixtures were analyzed using an Easy nLC nanoflow HPLC system (Proxeon Biosystems, Odense, Denmark; now Thermo Fisher Scientific) coupled via a nanoelectrospray ion source (Proxeon Biosystems) to an LTQ Orbitrap Velos mass spectrometer (35) (Thermo Fisher Scientific). Chromatographic peptide separation was done in a 20-cm chromatography column

(75-μm inner diameter) that was packed in-house with ReproSil-Pur C18-AQ 1.8-μm resin (Dr. Maisch GmbH, Ammerbuch-Entringen, Germany) in buffer A (0.5% acetic acid). The peptides were eluted at a flow rate of 200 nl/min with a linear gradient from 5% to 80% buffer B over 120 or 200 min depending on the experiment. At the end of the gradient, the column was washed with 90% buffer B and equilibrated with 5% buffer B. The source was operated at 2.1–2.2 kV, with no sheath gas flow and with the ion transfer tube at 200 °C.

The mass spectrometer was programmed to acquire in a data-dependent mode. For the "high-high" strategy, full scan MS spectra were acquired at a target value of 1,000,000 and a resolution of 30,000 at *m/z* 400 with lock mass option enabled for the 445.120025 ion in the Orbitrap analyzer. The ten most intense ions (signal threshold of 5,000 or 7,000) were sequentially isolated and accumulated to a target value of 40,000 with a maximum injection time of 150 ms and were fragmented by higher energy collisional dissociation (HCD) (35). Dynamic exclusion was defined by a list size of 500 features and exclusion duration of 60 or 120 ms. The spectra of the fragmented ions were acquired in the Orbitrap analyzer with resolution of 7,500 at *m/z* 400. Raw data (37 LC M/MS files) are deposited at Tranche (available at https://proteomecommons.org/tranche/ upon publication as "Proteome Analysis of Hsp90 Inhibition" via following hash code: 9oxlaZwptWe794CsZWQYC43zLsZ8TAO89CayUaRfSRpGy5wSEZC+p/D42vLstK1i6Xj4tqiMvOMryY5Uub8wl160kyoAAAAAABFhFw==).

Data Analysis—The raw MS data were processed and analyzed using the MaxQuant software (36) version 1.1.1.36. A false discovery rate of less than 0.01 for proteins, peptides, and phosphosites and a minimum peptide length of 6 amino acids were required. The mass accuracy of the precursor ions was improved by retention time-dependent mass recalibration (36). Andromeda (37) was used to search the peak lists against the International Protein Index human database 3.68 containing 87,061 entries combined with 248 frequently observed contaminants as well as reversed versions of all sequences.

Enzyme specificity was set to trypsin, additionally allowing cleavage N-terminal to proline and up to two missed cleavages. The search included cysteine carbamidomethylation as a fixed modification and *N*-acetylation of protein, oxidation of methionine, and phosphorylation of STY as variable modifications. Peptide identification was based on a search with an initial mass deviation of the precursor ion of up to 7 ppm, and the allowed fragment mass deviation was set to 20 ppm. Phosphorylation sites were assigned as previously described (38). To match identifications across different replicates and adjacent fractions, the "match between runs" option in MaxQuant was enabled within a time window of 2 min. Quantification of SILAC pairs was performed by MaxQuant with standard settings.

Bioinformatic Analysis—We based the annotation of proteins on Uniprot identifiers. Categorical annotation was supplied in the form of Gene Ontology (GO) biological process, molecular function, and cellular component, whereas pathway membership information was obtained from the KEGG database. We used the protein domain content from the PFAM database and protein fold information as defined by SCOP. The one-dimensional annotation matrix algorithm tests the difference of every protein annotation from the overall intensity distribution. This is done by ranking of the ratios and testing whether the proteins corresponding to every annotation term tend to be ranked higher or lower than the ranking of all proteins in the data set. The statistical test used is the two-sided Wilcoxon-Mann-Whitney test, a nonparametric test that is independent of the shape of the distribution. Because the number of terms and consequently the number of hypotheses tested simultaneously can become quite large, the multiple hypothesis testing is adjusted by applying a Benjamini-Hochberg false discovery rate threshold of 0.02.

The one-dimensional annotation analysis is more informative when computed on large numbers of entries per annotation term because of the statistical design of the analysis. Therefore, proteins with at least one quantification event were considered for one-dimensional annotation analysis (and histogram representations). Histograms for median normalized protein ratios between 17-DMAG-treated and control were plotted using the R statistical programming language. For calculation of correlation coefficients, data sets were filtered for entries with valid quantifications in all experiments. The proteins that passed the *t* test are summarized in supplemental Table 2, which also contains corresponding ratios in each replicate.

RESULTS

In Depth Proteome Coverage—To quantify 17-DMAG induced proteome changes in HeLa cells, we used SILAC-based quantitation and coupled it to high resolution LC MS/MS (Fig. 1*A*). A suitable concentration of 17-DMAG was found to be 50 μM, and proteomic changes were analyzed 24 h after drug treatment when protein level changes appeared to be strongest (supplemental Fig. 1). We analyzed five biological replicates where equal amounts of protein sample from control (untreated) and 17-DMAG-treated HeLa cell lysates were mixed and digested in solution with trypsin using the filter-aided sample preparation method, and the resulting peptides were fractionated by pipette-based strong anion exchange chromatography. The six peptide fractions from each replicate experiment were then analyzed by LC-MS/MS on a hybrid high resolution LTQ Orbitrap Velos using HCD-based fragmentation (Fig. 1*A*). The combined data set over five proteome replicates comprises 30 LC-MS/MS experiments with 4-h gradients. In contrast to the conventional "high-low" strategy, in which the fragments are measured in a linear ion trap, we obtained ppm range accuracy for both precursor ions and their fragments (a high-high strategy) by acquiring both the MS full scans and MS/MS fragmentation scans in the Orbitrap analyzer. As examples illustrating the data quality, Fig. 1*B* shows the HCD-based MS/MS spectrum of the doubly charged peptides of heat shock protein β1-Hsp27 and receptor tyrosine kinase-EGFR, which features the typical characteristics of extensive sequence coverage by y ions and a few low mass b ions (Fig. 1*B*). The high mass accuracy of the fragment ions is evident by the low ppm deviation for the Orbitrap measurements. More than 60% of the MS/MS scans were confidently identified, resulting in the identification of more than 7,000 proteins at a protein false discovery rate of less than 1% (supplemental Table 1). The protein identification were highly reproducible across replicates with more than 85% of proteins identified across at least three replicate experiments (Fig. 1*C*), thus providing us with an in depth proteome to assess the effects of 17-DMAG action.

Quantification of Proteome Changes—The data allowed accurate quantitative comparison of ~6,000 proteins in response to Hsp90 inhibition upon 17-DMAG treatment. A summary of the identification and quantification of proteins in the individual experiments is available in supplemental Table 1.

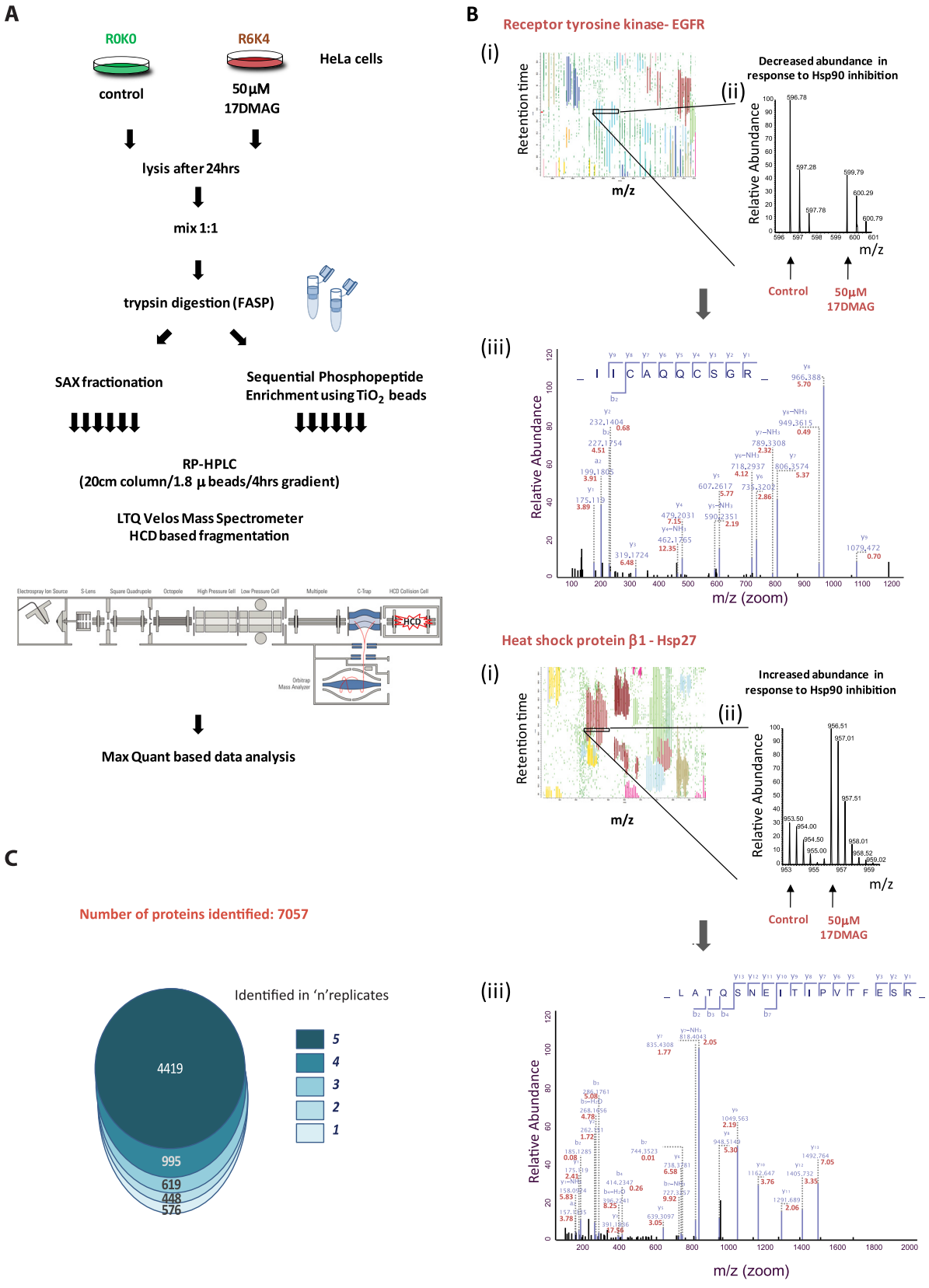
A
R0K0
R6K4
HeLa cells
control
50μM
17DMAG
lysis after 24hrs
mix 1:1
trypsin digestion (FASP)
SAX fractionation
Sequential Phosphopeptide
Enrichment using TiO2 beads
RP-HPLC
(20cm column/1.8 μ beads/4hrs gradient)
LTQ Velos Mass Spectrometer
HCD based fragmentation
Max Quant based data analysis
B
Receptor tyrosine kinase- EGFR
(i)
Retention time
m/z
(ii)
Decreased abundance in
response to Hsp90 inhibition
Relative Abundance
m/z
Control
50μM
17DMAG
(iii)
Relative Abundance
m/z (zoom)
Heat shock protein β1 - Hsp27
(i)
Retention time
m/z
(ii)
Increased abundance in
response to Hsp90 inhibition
Relative Abundance
m/z
Control
50μM
17DMAG
(iii)
Relative Abundance
m/z (zoom)
C
Number of proteins identified: 7057
Identified in 'n'replicates
4419
995
619
448
576
5
4
3
2
1

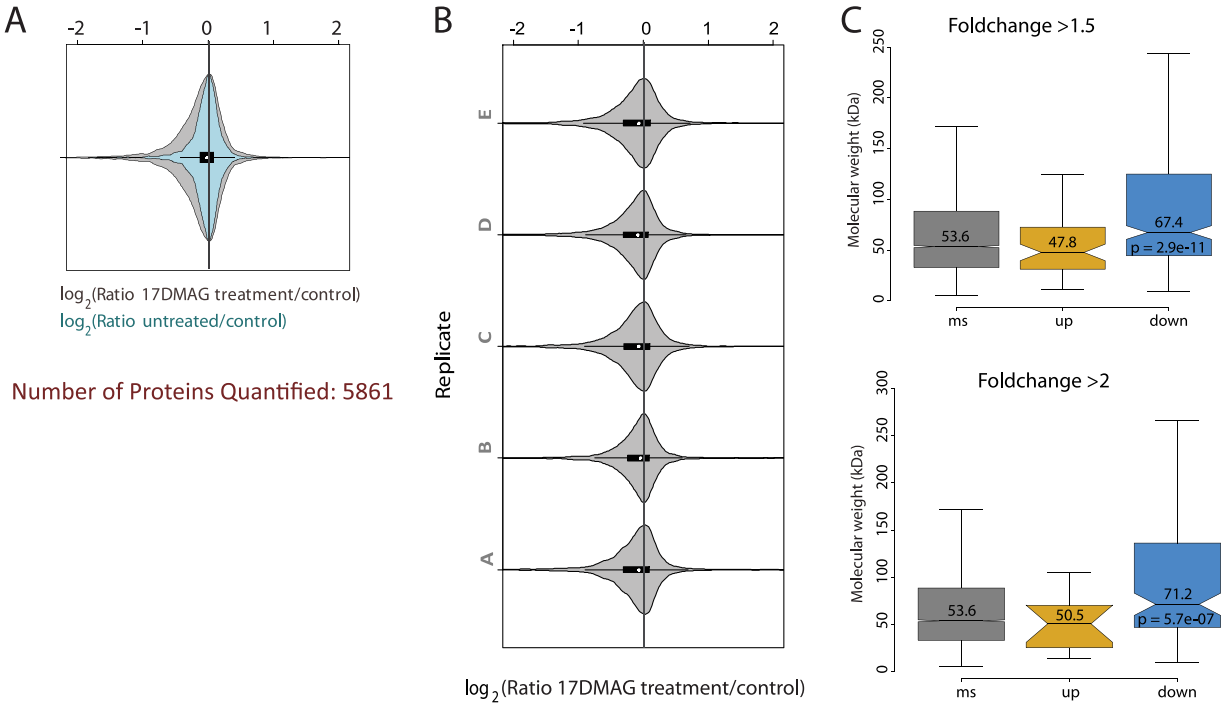

FIG. 2. **Quantified proteome: violin plot of the protein abundance ratios.** *A*, comparison between combined heat shock response data set (untreated control *versus* 17-DMAG treated HeLa cells) and technical variation (HeLa control 0 h *versus* 24 h). *B*, comparison between all five replicates for control *versus* 17-DMAG-treated HeLa cells. *C*, box plots indicating the distribution of molecular weights of identified proteins (*gray*), up-regulated (*gold*), and down-regulated (*blue*) by at least 1.5-fold (*upper box plot*) or 2-fold (*lower box plot*) change. The *bold horizontal line* indicates the median, and *whisker caps* indicate the 10th and 90th percentiles. *p* values are based on Mann-Whitney tests.

SILAC-based quantification of measured peptides is exemplified by peptides corresponding to EGFR and Hsp27, both of which are known to be affected after Hsp90 inhibition by 17-DMAG (Fig. 1*B*). Although EGFR is a client protein that is degraded in response to Hsp90 inhibition, Hsp27 is one of the heat shock proteins that are induced by HSF1 after this transcription factor is released from an inhibitory association with Hsp90 by 17-DMAG (17). We tested the reproducibility of our quantitative data by calculating the correlation between the five separately analyzed biological replicates and found a mean correlation between measurements of 0.78 (supplemental Fig. 2). We therefore conclude that our results are consistent and reproducible.

To obtain a global view of proteomic alterations, we analyzed the distribution of the log2 ratios of proteins between control and 17-DMAG-treated HeLa cells for the combined data set. For comparison, we obtained the biological and technical variation in a 1:1 mixture of the HeLa cell proteome after 24 h of culturing (Fig. 2*A*). In contrast to the control HeLa proteome, which approximates a normal and narrow distribution, a much broader ratio distribution of proteins (median averaged over biological replicates) was observed in re-

FIG. 1. **In depth quantitative proteomics of 17-DMAG-treated HeLa cells.** *A*, experimental strategy. Two cell populations of HeLa cells were SILAC-encoded by growing them in the presence of (light and heavy) stable isotope-labeled arginine and lysine. The heavy labeled population was incubated for the 24 h with 50 μM 17-DMAG, and the experiment was done in five replicates. Proteins were digested using filter-aided sample preparation, and peptides were fractionated by strong anion exchange (*SAX*) before analysis by high resolution mass spectrometry. For one replicate, the peptides were in parallel subjected to consecutive TiO_2 enrichment of phosphopeptides. Subsequently, all peptide and phosphopeptide mixtures were resolved by nanoLC and measured on an LTQ-Orbitrap Velos mass spectrometer using HCD. *B*, high accuracy at both the precursor mass and fragment levels (a high-high strategy) on the LTQ Orbitrap Velos. *Top left panel*, zoom of a typical part of the heat map of an LC MS/MS run of one of the peptide fractions obtained after strong anion exchange fractionation. Marks on the *left-hand side* represent the MS survey scans. *Top right panel*, MS spectrum of the representative peptides (doubly charged precursor shown in *blue*) from EGFR (IICAQQCSGR) or Hsp27 (LATQSNEITIPVTFESR) showing the isotope pattern of the SILAC pair. *Lower panel*, HCD-based MS/MS spectrum of the same peptide as in the *top right panel*. The peptides show nearly complete coverage by y ions and low mass b ions, and the characteristic a2,b2 ion pair is clearly visible. Mass deviation of fragment ions from calculated values in ppm is shown in *red*. The peptide intensities of the SILAC pairs are compared to obtain a quantitative map in response to 17-DMAG treatment. *C*, overlap in protein identification across biological replicates. The distribution of total number of proteins identified in the data set is shown as a function of their overlapping identification across *n* of the five biological replicates.

sponse to 17-DMAG treatment of HeLa cells. In addition, although the protein ratio distribution was unimodal, it was clearly asymmetric (Fig. 2*A*). When requiring a 1.5-fold change, 724 proteins (12.4%) showed decreased abundance and only 97 proteins (1.7%) increased abundance in response to Hsp90 inhibition. Similarly, at a 2-fold change, just 26 proteins (0.4%) were up-regulated, and 308 (5.3%) were down-regulated. The asymmetry in the protein ratio distribution was evident across all the measured replicates confirming the reproducibility of this observation (Fig. 2*B*). Hence we conclude that 17-DMAG treatment leads to more down-regulation because of the absence of chaperoning activity after Hsp90 inhibition than up-regulation because of HSF1 activation.

The effects of 17-DMAG may in part be due to inhibition of Grp94 (HSP90B1), the endoplasmic reticulum paralog of cytosolic Hsp90. Grp94 is an endoplasmic reticulum resident chaperone that is retained in the endoplasmic reticulum by a C-terminal KDEL sequence (39) and is involved in the folding/assembly of secretory proteins (such as immunoglobulins) and of several membrane proteins (40). It is known to be required for the cell surface expression of certain Toll-like receptors and integrins (41, 42). Grp94 is also inhibited by geldanamycin and derivatives (43), but little is known about the consequences of Grp94 inhibition, except that it elicits an ER stress response (43). To identify effects potentially caused by Grp94 inhibition, we analyzed the secretory proteins and the integral membrane proteins that were down-regulated upon treatment with 17-DMAG. As expected, we found only very few secretory proteins (115 proteins of a total of 6034 proteins quantified), because these leave the cells and would therefore be underrepresented in the analysis. 33 secretory proteins were ≥1.5-fold down-regulated in abundance upon 17-DMAG treatment. The number of membrane proteins (proteins with predicted transmembrane segments) in our analysis is 758, of which 94 were down-regulated ≥1.5-fold. 19 of these proteins are tyrosine kinase receptors or other proteins for which a role of cytosolic Hsp90 in folding has been established. Thus, at most 101 proteins are potentially affected by Grp94 inhibition in our study. In contrast, the number of ≥1.5-fold down-regulated proteins among the nonsecretory and nonmembrane proteins (5709 proteins in total) is ~600. Thus, we conclude that the vast majority of effects described are due directly or indirectly to inhibition of Hsp90. Potential Grp94 target proteins are marked in supplemental Table 2.

Analyzing the physicochemical properties of the proteins that decreased in abundance may provide insights into the structural determinants of Hsp90-client protein interactions. Proteins that passed the *t* test (supplemental Table 2) were analyzed for their molecular weight distribution at different fold change cutoffs. We noticed a small but very significant increase of the median molecular weight of the set of down-regulated or degraded proteins as compared with the whole group of identified proteins, in which it was 53.6 kDa: 67.4 kDa for at least 1.5-fold change and 71.2 kDa for at least 2-fold change (Fig. 2*C*). Notably, only one protein was larger than 250 kDa in the group of 1.5-fold up-regulated proteins, whereas the group of down-regulated proteins contained as many as 22 proteins larger than 250 kDa. Larger proteins may be less thermodynamically stable, and this metastability might become especially relevant under conditions of conformational stress.

Quantitative Changes in the Protein Folding Machinery—The paradigmatic effect of HSF1 activation resulting from Hsp90 inhibition is the accumulation of heat shock proteins, also called molecular chaperones. They assist in protein folding and prevent protein misfolding and aggregation, and they constituted the most significantly up-regulated protein class upon Hsp90 inhibition (supplemental Table 2). For example, several members of the Hsp70 family were found to accumulate. Interestingly, a constitutive heat shock cognate protein, HSC70, was consistently up-regulated as well. Whether this latter effect is specific for a tumor cell line needs to be further clarified (44). In addition, our data contain at least seven different DnaJ (Hsp40) class co-chaperones up-regulated upon Hsp90 inactivation. Hsp40 co-chaperones are known to adapt the functionality of Hsp70s to specific cellular needs, such as different target substrates or cellular locations (45). Thus, the transcriptional activation of the cytosolic stress response resulting from Hsp90 inhibition provides the cell with the capacity to deal with a wide range of misfolding proteins.

The induction of chaperones by HSF1 is considered to constitute a negative feedback loop, whereby newly translated Hsp90 accumulates to a level where it can rebind and thus inactivate HSF1. Indeed, we found that 24 h after Hsp90 inhibition, the abundance of both isoforms of Hsp90 increased. In addition, some co-chaperones of the Hsp90 folding cycle, such as Aha1 (gene name AHSA1) and Hop1 (gene name STIP1) (46), increased as well.

HSF1 Dependence of Cellular Reaction—Our finding that Hsp90 inactivation affected diverse cellular processes supports the current view that the Hsp90-controlled transcription factor HSF1 is involved in the regulation of more than only heat shock proteins (47). Indeed, in addition to molecular chaperones, a number of HSF1-controlled genes were activated by Hsp90 inhibition. To perform this analysis systematically, we used a list of experimentally determined HSF1-controlled genes (48). We found that in addition to chaperones, approximately a quarter (15 of 64) of the proteins that were at least 1.5-fold and significantly up-regulated correspond to genes described in the above study as directly depending on HSF1. This may suggest that a core of HSF1-induced genes drives a more extensive, indirect cellular reaction needed to adjust to stress. Remarkably, 9 of 13 of the 2-fold up-regulated proteins are already known HSF1 targets, attesting to the specificity and accuracy of our data set.

Bioinformatic Analysis of 17-DMAG Inhibition—To functionally understand the differences in protein expression levels between two proteomes, one can divide a histogram of quantitative expression changes into quantiles. Each quantile can then be tested separately for enrichment of every annotation term (such as KEGG pathways, GO biological processes, and PFAM domains) to find whether the corresponding expression ratios have a preference to be systematically larger or smaller than the global distribution of the values for all proteins (22).

Here we used a generalized concept to the above quantile analysis, termed one-dimensional enrichment analysis (49). Although similar to the quantile-based enrichment calculations, the one-dimensional annotation enrichment employed here to analyze the functional differences between 17-DMAG-treated and control proteome has the advantage that it is not necessary to define an arbitrary positioning of quantiles or regulation cutoffs beforehand. Instead, the distribution of values is scanned for interesting subcategories in an unbiased way. For those categories that are significant, a position score (termed "*s*," a number between −1 and 1) is calculated, indicating where the center of the distribution of values for the protein category is located relative to the overall distribution of values. A value near 1 indicates that the protein category is strongly concentrated at the high end of the ratio distribution (up-regulation), whereas a value near −1 means that the values are all at the low end of the distribution (down-regulation).

Pathways and Processes Affected by 17-DMAG Inhibition—The one-dimensional annotation analysis of ratios of protein abundances upon 17-DMAG treatment was carried out for various protein annotation terms including GO categories (biological processes, cellular compartment and molecular function), KEGG pathways, PFAM domains, and SCOP folds (supplemental Table 3). Focusing specifically on the annotation terms linked to KEGG pathways in this analysis, we found that the most significant KEGG pathways enriched after Hsp90 inhibition were the proteasome, with a positive score indicating up-regulation of protein members, and nucleotide excision repair pathway, with a negative score indicating down-regulation of this biological process (supplemental Fig. 3 and supplemental Table 3). Mechanistically, this is readily explained by the fact that Hsp90 inhibition by 17-DMAG prominently leads to ubiquitination and eventual proteasomal degradation of its client proteins. Furthermore, it has already been shown that 17-DMAG interferes with base excision repair pathway, thereby synergizing with irradiation of lung cancer cells (50). Nevertheless, the fact that these pathways are so clearly identified in the one-dimensional annotation analysis makes them excellent positive controls for our quantitative proteomics approach. Other significantly down-regulated pathways include sphingolipid metabolism, which would be interesting to explore given that this pathway has been implicated in cancer (reviewed in Refs. 51 and 52). Its alteration by 17-DMAG treatment has not been reported so far in connection with mechanisms of anticancer properties of Hsp90 inhibitors.

The quantitative proteomic differences between control and 17-DMAG-treated HeLa cells were further analyzed by one-dimensional annotation analysis to provide a functional portrait of drug action. As shown in Fig. 3*A* and supplemental Table 3, the most significantly enriched categories with a positive score difference are composed of proteins associated with protein folding, unfolded protein binding, and response to unfolded protein. The induced proteins in these categories are mostly molecular chaperones and proteases, hallmarks of activation of a heat shock response, which can then refold misfolded proteins or degrade irreparably damaged polypeptides, respectively. For instance, HSF1-dependent Hsp70 and Hsp27 induction frequently occurs in response to Hsp90 inhibitor treatment. The log2 ratio distribution of proteins belonging to these categories was systematically larger than the global distribution of the values for all quantified proteins (Fig. 3*B*).

Intriguingly, the two most significantly down-regulated functional categories included "DNA metabolic process" and "protein kinase activity" ($p < 10^{-13}$). A moderately negative value of differences for these categories with many members indicates that there is a significant collective shift toward lower expression ratios in response to Hsp90 inhibition for this category, which, however, may be small in absolute terms and possibly not noticeable when looking at individual proteins. Such statistically significant enrichment of specific functional categories indicates a "tailored" response to Hsp90 inhibition (Fig. 3).

The enrichment of DNA metabolic processes corresponds to down-regulation of proteins associated with GO biological process categories such as "cellular response to DNA damage," "DNA modification," "response to DNA damage stimulus," and "regulation of transcription" and GO molecular function categories such as "DNA binding," "sequence-specific DNA binding," and "transcription regulator activity" (supplemental Table 3). The down-regulation of these categories is in agreement with earlier observations that increased levels of Hsp90 frequently compromise the effects of radiotherapy and that Hsp90 inhibitors affect nucleotide excision repair (53). Indeed, Hsp90 clients include proteins conferring radiation resistance and their down-regulation by Hsp90 inhibitors is therefore accompanied by an increase in radiosensitivity. This radiosensitization has been linked to compromised DNA damage response to radiation, including the inhibition of cell cycle checkpoint activation and DNA double-strand break repair (50).

Effects on the Kinome—The one-dimensional analysis of the quantitative proteomic map highlighted the kinome. *i.e.* the class of protein kinases, as one of the two most significantly down-regulated functional categories in response to 17-DMAG treatment. For protein kinase activity and associated categories, the *s* value was moderate at −0.28, but the significance value was very high ($p < 10^{-13}$). This indicates that upon Hsp90 inhibition, the kinome collectively shifts to-

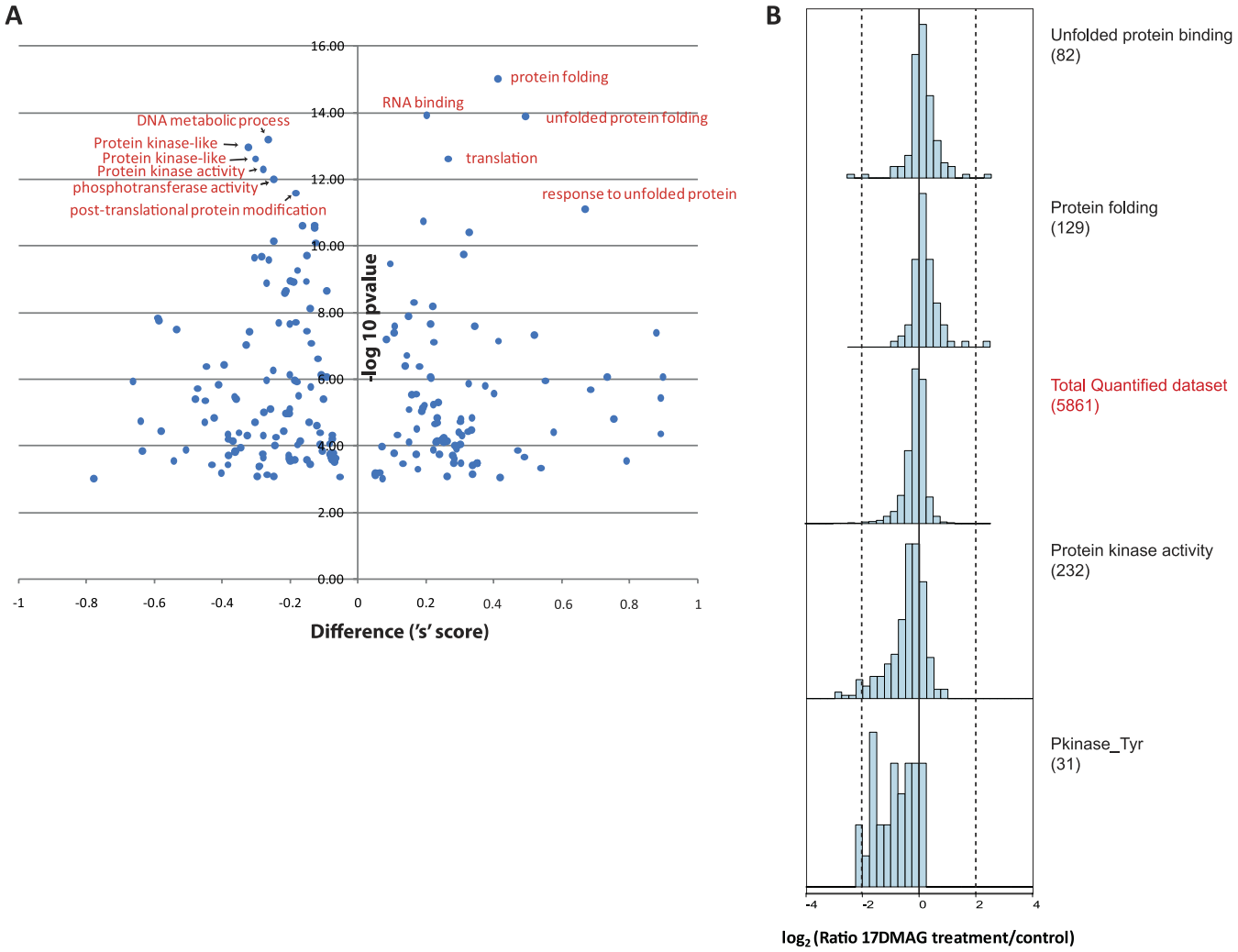

FIG. 3. **One-dimensional annotation analysis: heat shock response *versus* the control HeLa cell line.** *A*, annotation terms (KEGG, GO, PFAM, and SCOP) of proteins significantly altered during stress response. The ratios for the proteins corresponding to these terms show a tendency to be systematically different from the global distribution of the ratios for all proteins as indicated by the difference score *s*. The data points corresponding to annotation terms whose members are regulated with a very high significance inhibition are labeled ($p < 10^{-11}$). *B*, histogram of all log2 protein ratios between 17-DMAG-treated *versus* control HeLa proteome is shown in the *middle panel*, and ratios for proteins belonging to the most significantly affected annotation categories (marked next to the histogram) are displayed *above* and *below*.

ward lower expression ratios (Fig. 3). Because kinases are generally low abundance proteins, which are often specifically enriched for detailed proteomic analysis (54), we examined their representation in the data set. Across the five replicate proteome measurements, we identified 276 kinases, and 215 of them were quantified in at least one experiment, whereas 178 were quantified in at least three experiments. Among these 178 kinases, 60 were significantly and reproducibly reduced 1.25-fold, and 41 were reduced more than 1.5-fold. The abundance of 23 kinases (13%) decreased by more than half (supplemental Table 4). The down-regulated kinases included at least 23 known client protein kinases of Hsp90 such as AKT1, WEE1, EGFR, EPHA2, and CDK4 (55, 56). Interestingly, CSNK1A1 was recently identified as one of the kinases forming Hsp90 interactions (24). The fact that we found its level reduced after 17-DMAG treatment further strengthens the probability that the down-regulated kinases are Hsp90 client proteins.

To gain insight into the selectivity of the drug toward kinome subsets, we mapped the distribution of protein kinases across the human kinome dendogram that were down-regulated by more than 1.5-fold after Hsp90 inhibition (Fig. 4*B*). A number of tyrosine kinases were evident in this analysis. Furthermore, by one-dimensional annotation analysis of the enriched protein functional domains and GO molecular function, we found that the protein tyrosine kinase subset exhibited a higher extent of down-regulation ($s = -0.58$) compared with the total kinome ($s = -0.28$) (Figs. 3*B* and 4*A* and supplemental Table 3).

Effects on the Phosphoproteome—The down-regulation of the kinome in response to Hsp90 inhibition prompted us to

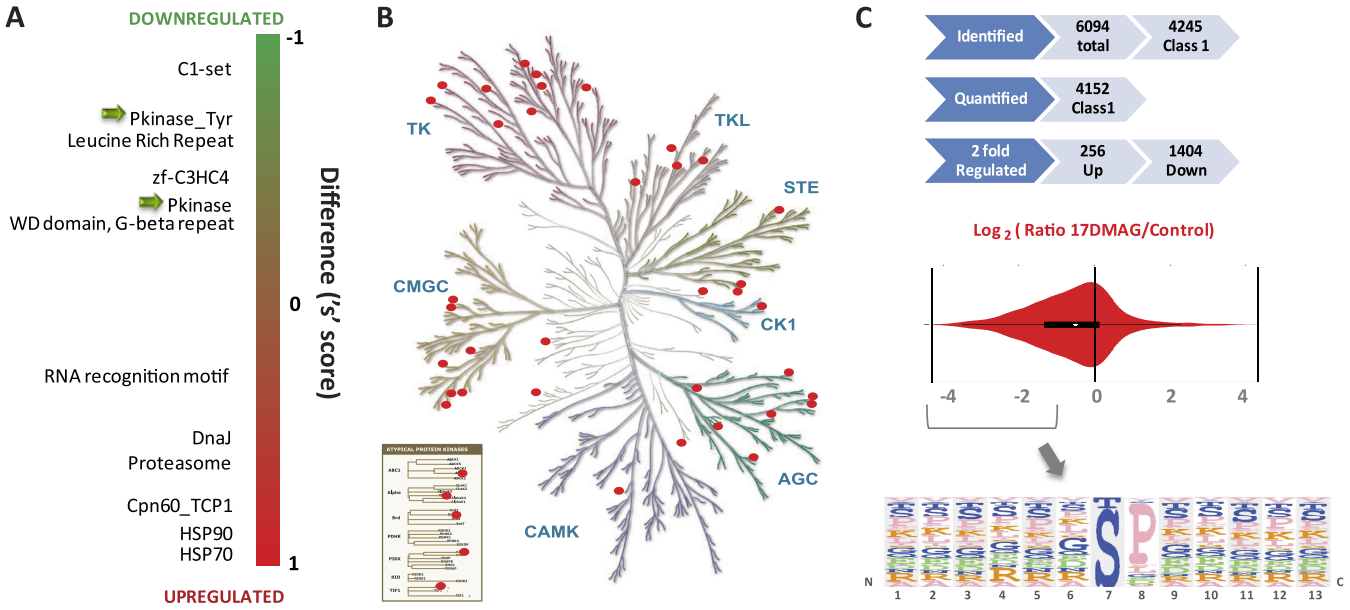

FIG. 4. **Hsp90 inhibition and protein kinases.** *A*, one-dimensional annotation enrichment analyses for PFAM terms are shown on a difference score *s* axis, and significantly enriched terms are indicated. *B*, the protein kinases whose abundance is reduced by at least 1.5-fold in response to Hsp90 inhibition are marked in the dendrogram of the human kinome. *AGC*, protein kinase A, G, and C families; *CMGC*, CDK, MAPK, GSK3, and CLK family; *CAMK*, calmodulin/calcium-regulated kinases; *CK1*, cell kinase 1; *STE*, homologs of the yeast STE; *TK*, tyrosine kinase; *TKL*, tyrosine kinase-like. Reproduced with permission from the American Association of Science. *C*, quantitative phosphoproteomics analysis. The *top panel* provides a summary of number of phosphosites identified and quantified in the data set and those regulated in response to Hsp90 inhibition. The *middle panel* shows log2 ratio distribution for phosphosites between 17-DMAG-treated *versus* untreated HeLa control. The *bottom panel* shows the frequency plot for motif enrichment of the down-regulated phosphorylation sites.

investigate possible consequences on the phosphoproteome. We reasoned that the suppression of kinase abundance induced by the Hsp90 inhibitor 17-DMAG should become apparent as a decrease in kinase-mediated phosphorylation events. Following the same experimental design as for mapping the proteome alterations (Fig. 1), we probed the quantitative phosphoproteomic changes in response to Hsp90 inhibition in HeLa cells that were labeled with heavy forms of arginine and lysine.

We used incubation with TiO_2 beads, both as an enrichment and a fractionation method for phosphopeptides, and subjected the peptide mix to seven consecutive TiO_2 enrichments. Mass spectrometric data from the phosphoproteome data set was processed in the MaxQuant environment using stringent criteria (false discovery rate at the peptide, localization, and protein levels < 0.01; "Experimental Procedures"). We identified more multiply phosphorylated peptides enriched at high peptide to bead ratio in the first six consecutive enrichments, whereas singly phosphorylated peptides were identified in the last enrichment steps with a low peptide-to-bead ratio (supplemental Fig. 4), as has been reported before (32). We identified more than 6,000 phosphosites and quantified more than 4,000 class 1 phosphosites that could be localized with high accuracy to particular serine, threonine, or tyrosine residues (average localization probability 0.97) (supplemental Table 5). The response pattern of the phosphoproteome to Hsp90 inhibitor treatment is apparent in the log2 ratio distribution of the quantified phosphoproteomic data set (Fig. 4*C*). It is highly asymmetric (~6% up *versus* ~34% down by more than 2-fold) and thereby clearly reveals a strong, system wide preference for down-regulation of cellular phosphorylation events. This is readily explained as a generic decrease in cellular phosphorylation events caused by the above described decreased abundance of Hsp90 client kinases after the inhibitor treatment. The exact series of causation is difficult to disentangle but is probably a combination of primary as well as secondary effects of the perturbed kinome.

Next, we analyzed the sequences of ~1500 phosphosites that were at least 2-fold down-regulated using the Perseus part of the MaxQuant computational proteomics environment (Fig. 4*C*, *lower panel*). The resulting frequency plots revealed that more than half of the down-regulated phosphorylation events contain "proline-directed" motifs. This motif mainly represents the consensus amino acid sequence for substrates of mitogen-activated or cyclin-dependent kinases (57, 58). This predominance of proline-directed motifs may be attributable to a decrease in abundance of cyclin-dependent kinases (CDK4 and CDK11, both previously known Hsp90 substrates, and of CDK5 and CDK12 identified here), as well as to reduced MAPK signaling, a common downstream pathway for many signaling pathways including those affected by 17-DMAG.

DISCUSSION

Here we have performed the first systematic study of the effect of Hsp90 inhibition on proteome composition using the Hsp90 inhibitor 17-DMAG. Our analysis provides a rich resource for further studies on the effect of Hsp90 inhibitors. The drug response turned out to be rather tailored, specifically activating a heat shock response and targeting DNA metabolic processes, the kinome, and its associated phosphoproteome. Our identification of a large number of protein kinases as client proteins of the Hsp90 chaperone system relied on obtaining an in depth quantification of the proteome with multiple replicates. As a consequence, the quantitative map obtained in this study allows us to clearly pinpoint protein kinases as one of the prime effectors of drug action. The specific effect of the Hsp90 inhibitor on the kinome could explain, at least in part, the preclinical observation that Hsp90 inhibitors abrogate oncogene switching that otherwise allows cancer cells to signal through different oncogenic kinases when one of them is blocked. This is an important mechanism of tumor escape from targeted kinase inhibitors, resulting in drug resistance, and the main reason behind the increasing popularity of applying Hsp90 inhibitors in combination with targeted kinase inhibitors (59–61).

Although it was known that inhibition of Hsp90 induces the stress response and that a number of kinases utilize Hsp90 for folding and regulation (7), the proteome-wide effects of Hsp90 inhibitors have never been assessed. We identified and extended the repertoire of proteins whose levels are affected in response to 17-DMAG-mediated Hsp90 inhibition even in highly explored protein classes such as protein tyrosine kinases. For example, we found that 17-DMAG down-regulates ROR2 (Wnt receptor), a tyrosine kinase that can either promote or suppress tumor formation, depending on tumor type and molecular context. ROR2 is overexpressed in oral and renal cancer, as well as in osteosarcoma. Its overexpression activates JNK (noncanonical Wnt pathway) and has pro-tumorigenic effects (62, 63). Conversely, it has been reported that in colon cancer cells, constitutive Wnt signaling leads to tumorigenesis, and epigenetic repression of ROR2 has a Wnt-mediated, pro-tumorigenic role (64, 65).

One of the non-heat shock proteins that were up-regulated after Hsp90 inhibition was ADAMTS1 (disintegrin and metalloproteinase with thrombospondin motifs 1). This is interesting, because the up-regulation was relatively large (2.5-fold) and because ADAMTS1 has been shown to exert angioinhibitory properties by interacting with vascular endothelial growth factor A (66). Thus, this up-regulation could contribute to the anticancer properties of 17-DMAG.

Clearly, not all of the proteome changes observed in response to Hsp90 inhibition have anticancer properties, and some critical signaling molecules are even affected in an undesired way. For example, LRIG1, a proposed tumor suppressor and feedback attenuator of RTK signaling is down-regulated upon 17-DMAG treatment. LRIG1 down-regulation has been observed in several cancers, including renal cell carcinoma and breast cancer, and in several cancer cell lines (67–69). Tumor-associated antigen L6 (TM4SF1), a key regulator of pathologic angiogenesis *in vivo* involved in cancer invasion and metastasis (70), was also found to be up-regulated. It was expected to find some of these undesirable targets, given the broad cellular effects of Hsp90 inhibition. Indeed, although the clinical effects of Hsp90 inhibitors as anticancer agents are promising in some situations, this strategy appears to be ineffective in other settings. In this regard, our data and observations may be useful in guiding the therapeutic applications of 17-DMAG and similar drugs in cancer therapy. The wide-ranging up-regulation of molecular chaperones and stress proteins by 17-DMAG must also be regarded as an undesired property of an anti-cancer drug, because higher chaperone levels contribute to sustaining the growth of cancer cells (6). However, the efficiency of 17-DMAG to activate the chaperone system may be useful in the treatment of diseases associated with protein misfolding and aggregation (12). The systems-wide proteomic strategy developed here should prove useful in the evaluation of drug effects and improving the selection of drug combinations.

Acknowledgments—We thank Christian Eberl and Rochelle C. J. D'souza for helpful discussions and Korbinian Mayr for technical support.

* This work was supported by European Commission's 7th Framework Program PROSPECTS Grant Agreement HEALTH-F4-2008-201648. The costs of publication of this article were defrayed in part by the payment of page charges. This article must therefore be hereby marked "*advertisement*" in accordance with 18 U.S.C. Section 1734 solely to indicate this fact.

S This article contains supplemental material.

§ These authors contributed equally to this work.

‖ Present address: Frankfurt Institute for Molecular Life Sciences and Institute of Biophysical Chemistry, Goethe University Frankfurt, Max-von-Laue-Str.15, 60438 Frankfurt am Main, Germany.

** Present address: Proteom Centrum Tübingen, Auf der Morgenstelle 15, 72076 Tübingen, Germany.

‡‡ To whom correspondence may be addressed. Tel.: 49-89-8578-2557; E-mail: mmann@biochem.mpg.de.

§§ To whom correspondence may be addressed. Tel.: 49-89-8578-2244; E-mail: uhartl@biochem.mpg.de.

REFERENCES

1. Hartl, F. U., Bracher, A., and Hayer-Hartl, M. (2011) Molecular chaperones in protein folding and proteostasis. *Nature* **475,** 324–332
2. Klettner, A. (2004) The induction of heat shock proteins as a potential strategy to treat neurodegenerative disorders. *Drug News Perspect.* **17,** 299–306
3. Broadley, S. A., and Hartl, F. U. (2009) The role of molecular chaperones in human misfolding diseases. *FEBS Lett.* **583,** 2647–2653
4. Muchowski, P. J., and Wacker, J. L. (2005) Modulation of neurodegeneration by molecular chaperones. *Nat. Rev. Neurosci.* **6,** 11–22
5. Evans, C. G., Chang, L., and Gestwicki, J. E. (2010) Heat shock protein 70 (Hsp70) as an emerging drug target. *J. Med. Chem.* **53,** 4585–4602
6. Santagata, S., Hu, R., Lin, N. U., Mendillo, M. L., Collins, L. C., Hankinson, S. E., Schnitt, S. J., Whitesell, L., Tamimi, R. M., Lindquist, S., and Ince, T. A. (2011) High levels of nuclear heat-shock factor 1 (HSF1) are asso-

ciated with poor prognosis in breast cancer. *Proc. Natl. Acad. Sci. U.S.A.* **108,** 18378–18383
7. Taipale, M., Jarosz, D. F., and Lindquist, S. (2010) HSP90 at the hub of protein homeostasis: Emerging mechanistic insights. *Nat. Rev. Mol. Cell Biol.* **11,** 515–528
8. Whitesell, L., Mimnaugh, E. G., De Costa, B., Myers, C. E., and Neckers, L. M. (1994) Inhibition of heat shock protein HSP90-pp60v-src heteroprotein complex formation by benzoquinone ansamycins: Essential role for stress proteins in oncogenic transformation. *Proc. Natl. Acad. Sci. U.S.A.* **91,** 8324–8328
9. Trepel, J., Mollapour, M., Giaccone, G., and Neckers, L. (2010) Targeting the dynamic HSP90 complex in cancer. *Nat. Rev. Cancer* **10,** 537–549
10. Zou, J., Guo, Y., Guettouche, T., Smith, D. F., and Voellmy, R. (1998) Repression of heat shock transcription factor HSF1 activation by HSP90 (HSP90 complex) that forms a stress-sensitive complex with HSF1. *Cell* **94,** 471–480
11. Stebbins, C. E., Russo, A. A., Schneider, C., Rosen, N., Hartl, F. U., and Pavletich, N. P. (1997) Crystal structure of an Hsp90-geldanamycin complex: Targeting of a protein chaperone by an antitumor agent. *Cell* **89,** 239–250
12. Sittler, A., Lurz, R., Lueder, G., Priller, J., Lehrach, H., Hayer-Hartl, M. K., Hartl, F. U., and Wanker, E. E. (2001) Geldanamycin activates a heat shock response and inhibits huntingtin aggregation in a cell culture model of Huntington's disease. *Hum. Mol. Genet.* **10,** 1307–1315
13. Burger, A. M., Fiebig, H. H., Stinson, S. F., and Sausville, E. A. (2004) 17-(Allylamino)-17-demethoxygeldanamycin activity in human melanoma models. *Anticancer Drugs* **15,** 377–387
14. Sepp-Lorenzino, L., Ma, Z., Lebwohl, D. E., Vinitsky, A., and Rosen, N. (1995) Herbimycin A induces the 20 S proteasome- and ubiquitin-dependent degradation of receptor tyrosine kinases. *J. Biol. Chem.* **270,** 16580–16587
15. Sharp, S., and Workman, P. (2006) Inhibitors of the HSP90 molecular chaperone: Current status. *Adv. Cancer Res.* **95,** 323–348
16. Schneider, C., Sepp-Lorenzino, L., Nimmesgern, E., Ouerfelli, O., Danishefsky, S., Rosen, N., and Hartl, F. U. (1996) Pharmacologic shifting of a balance between protein refolding and degradation mediated by Hsp90. *Proc. Natl. Acad. Sci. U.S.A.* **93,** 14536–14541
17. Whitesell, L., and Lindquist, S. L. (2005) HSP90 and the chaperoning of cancer. *Nat. Rev. Cancer* **5,** 761–772
18. Sleno, L., and Emili, A. (2008) Proteomic methods for drug target discovery. *Curr. Opin. Chem. Biol.* **12,** 46–54
19. Walgren, J. L., and Thompson, D. C. (2004) Application of proteomic technologies in the drug development process. *Toxicol. Lett.* **149,** 377–385
20. Bantscheff, M., Eberhard, D., Abraham, Y., Bastuck, S., Boesche, M., Hobson, S., Mathieson, T., Perrin, J., Raida, M., Rau, C., Reader, V., Sweetman, G., Bauer, A., Bouwmeester, T., Hopf, C., Kruse, U., Neubauer, G., Ramsden, N., Rick, J., Kuster, B., and Drewes, G. (2007) Quantitative chemical proteomics reveals mechanisms of action of clinical ABL kinase inhibitors. *Nat. Biotechnol.* **25,** 1035–1044
21. Sharma, K., Weber, C., Bairlein, M., Greff, Z., Kéri, G., Cox, J., Olsen, J. V., and Daub, H. (2009) Proteomics strategy for quantitative protein interaction profiling in cell extracts. *Nat. Methods* **6,** 741–744
22. Pan, C., Olsen, J. V., Daub, H., and Mann, M. (2009) Global effects of kinase inhibitors on signaling networks revealed by quantitative phosphoproteomics. *Mol. Cell. Proteomics* **8,** 2796–2808
23. Zhao, R., Davey, M., Hsu, Y. C., Kaplanek, P., Tong, A., Parsons, A. B., Krogan, N., Cagney, G., Mai, D., Greenblatt, J., Boone, C., Emili, A., and Houry, W. A. (2005) Navigating the chaperone network: An integrative map of physical and genetic interactions mediated by the hsp90 chaperone. *Cell* **120,** 715–727
24. Gano, J. J., and Simon, J. A. (2010) A proteomic investigation of ligand-dependent HSP90 complexes reveals CHORDC1 as a novel ADP-dependent HSP90-interacting protein. *Mol. Cell. Proteomics* **9,** 255–270
25. Schumacher, J. A., Crockett, D. K., Elenitoba-Johnson, K. S., and Lim, M. S. (2007) Proteome-wide changes induced by the Hsp90 inhibitor, geldanamycin in anaplastic large cell lymphoma cells. *Proteomics* **7,** 2603–2616
26. Maloney, A., Clarke, P. A., Naaby-Hansen, S., Stein, R., Koopman, J. O., Akpan, A., Yang, A., Zvelebil, M., Cramer, R., Stimson, L., Aherne, W., Banerji, U., Judson, I., Sharp, S., Powers, M., deBilly, E., Salmons, J., Walton, M., Burlingame, A., Waterfield, M., and Workman, P. (2007) Gene and protein expression profiling of human ovarian cancer cells treated with the heat shock protein 90 inhibitor 17-allylamino-17-demethoxygeldanamycin. *Cancer Res.* **67,** 3239–3253
27. Ong, S. E., Blagoev, B., Kratchmarova, I., Kristensen, D. B., Steen, H., Pandey, A., and Mann, M. (2002) Stable isotope labeling by amino acids in cell culture, SILAC, as a simple and accurate approach to expression proteomics. *Mol. Cell. Proteomics* **1,** 376–386
28. Wiśniewski, J. R., Zougman, A., Nagaraj, N., and Mann, M. (2009) Universal sample preparation method for proteome analysis. *Nat. Methods* **6,** 359–362
29. Wiśniewski, J. R., Zougman, A., and Mann, M. (2009) Combination of FASP and StageTip-based fractionation allows in-depth analysis of the hippocampal membrane proteome. *J. Proteome Res.* **8,** 5674–5678
30. Rappsilber, J., Ishihama, Y., and Mann, M. (2003) Stop and go extraction tips for matrix-assisted laser desorption/ionization, nanoelectrospray, and LC/MS sample pretreatment in proteomics. *Anal. Chem.* **75,** 663–670
31. Pinkse, M. W., Uitto, P. M., Hilhorst, M. J., Ooms, B., and Heck, A. J. (2004) Selective isolation at the femtomole level of phosphopeptides from proteolytic digests using 2D-NanoLC-ESI-MS/MS and titanium oxide precolumns. *Anal. Chem.* **76,** 3935–3943
32. Li, Q. R., Ning, Z. B., Tang, J. S., Nie, S., and Zeng, R. (2009) Effect of peptide-to-TiO_2 beads ratio on phosphopeptide enrichment selectivity. *J. Proteome Res.* **8,** 5375–5381
33. Larsen, M. R., Thingholm, T. E., Jensen, O. N., Roepstorff, P., and Jørgensen, T. J. (2005) Highly selective enrichment of phosphorylated peptides from peptide mixtures using titanium dioxide microcolumns. *Mol. Cell. Proteomics* **4,** 873–886
34. Macek, B., Mann, M., and Olsen, J. V. (2009) Global and site-specific quantitative phosphoproteomics: Principles and applications. *Annu. Rev. Pharmacol. Toxicol.* **49,** 199–221
35. Olsen, J. V., Schwartz, J. C., Griep-Raming, J., Nielsen, M. L., Damoc, E., Denisov, E., Lange, O., Remes, P., Taylor, D., Splendore, M., Wouters, E. R., Senko, M., Makarov, A., Mann, M., and Horning, S. (2009) A dual pressure linear ion trap Orbitrap instrument with very high sequencing speed. *Mol. Cell. Proteomics* **8,** 2759–2769
36. Cox, J., and Mann, M. (2008) MaxQuant enables high peptide identification rates, individualized p.p.b.-range mass accuracies and proteome-wide protein quantification. *Nat. Biotechnol.* **26,** 1367–1372
37. Cox, J., Neuhauser, N., Michalski, A., Scheltema, R. A., Olsen, J. V., and Mann, M. (2011) Andromeda: A peptide search engine integrated into the MaxQuant environment. *J. Proteome Res.* **10,** 1794–1805
38. Olsen, J. V., Blagoev, B., Gnad, F., Macek, B., Kumar, C., Mortensen, P., and Mann, M. (2006) Global, *in vivo*, and site-specific phosphorylation dynamics in signaling networks. *Cell* **127,** 635–648
39. Borgese, N., Francolini, M., and Snapp, E. (2006) Endoplasmic reticulum architecture: Structures in flux. *Curr. Opin. Cell Biol.* **18,** 358–364
40. Melnick, J., Dul, J. L., and Argon, Y. (1994) Sequential interaction of the chaperones BiP and GRP94 with immunoglobulin chains in the endoplasmic reticulum. *Nature* **370,** 373–375
41. Yang, Y., Liu, B., Dai, J., Srivastava, P. K., Zammit, D. J., Lefrançois, L., and Li, Z. (2007) Heat shock protein gp96 is a master chaperone for toll-like receptors and is important in the innate function of macrophages. *Immunity* **26,** 215–226
42. Liu, B., and Li, Z. (2008) Endoplasmic reticulum HSP90b1 (gp96, grp94) optimizes B-cell function via chaperoning integrin and TLR but not immunoglobulin. *Blood* **112,** 1223–1230
43. Lawson, B., Brewer, J. W., and Hendershot, L. M. (1998) Geldanamycin, an hsp90/GRP94-binding drug, induces increased transcription of endoplasmic reticulum (ER) chaperones via the ER stress pathway. *J. Cell. Physiol.* **174,** 170–178
44. Dai, C., Whitesell, L., Rogers, A. B., and Lindquist, S. (2007) Heat shock factor 1 is a powerful multifaceted modifier of carcinogenesis. *Cell* **130,** 1005–1018
45. Kampinga, H. H., and Craig, E. A. (2010) The HSP70 chaperone machinery: J proteins as drivers of functional specificity. *Nat. Rev. Mol. Cell Biol.* **11,** 579–592
46. Wandinger, S. K., Richter, K., and Buchner, J. (2008) The Hsp90 chaperone machinery. *J. Biol. Chem.* **283,** 18473–18477
47. Akerfelt, M., Morimoto, R. I., and Sistonen, L. (2010) Heat shock factors:

Integrators of cell stress, development and lifespan. *Nat. Rev. Mol. Cell Biol.* **11,** 545–555
48. Page, T. J., Sikder, D., Yang, L., Pluta, L., Wolfinger, R. D., Kodadek, T., and Thomas, R. S. (2006) Genome-wide analysis of human HSF1 signaling reveals a transcriptional program linked to cellular adaptation and survival. *Mol. Biosyst.* **2,** 627–639
49. Cox, J., and Mann, M. (2012) 2D annotation enrichment: A statistical method integrating quantitative proteomics with complementary high-throughput data. *BMC Bioinformatics,* in revision
50. Koll, T. T., Feis, S. S., Wright, M. H., Teniola, M. M., Richardson, M. M., Robles, A. I., Bradsher, J., Capala, J., and Varticovski, L. (2008) HSP90 inhibitor, DMAG, synergizes with radiation of lung cancer cells by interfering with base excision and ATM-mediated DNA repair. *Mol. Cancer Ther.* **7,** 1985–1992
51. Oskouian, B., and Saba, J. D. (2010) Cancer treatment strategies targeting sphingolipid metabolism. *Adv. Exp. Med. Biol.* **688,** 185–205
52. Ponnusamy, S., Meyers-Needham, M., Senkal, C. E., Saddoughi, S. A., Sentelle, D., Selvam, S. P., Salas, A., and Ogretmen, B. (2010) Sphingolipids and cancer: Ceramide and sphingosine-1-phosphate in the regulation of cell death and drug resistance. *Future Oncol.* **6,** 1603–1624
53. Dote, H., Burgan, W. E., Camphausen, K., and Tofilon, P. J. (2006) Inhibition of hsp90 compromises the DNA damage response to radiation. *Cancer Res.* **66,** 9211–9220
54. Sharma, K., Kumar, C., Kéri, G., Breitkopf, S. B., Oppermann, F. S., and Daub, H. (2010) Quantitative analysis of kinase-proximal signaling in lipopolysaccharide-induced innate immune response. *J. Proteome Res.* **9,** 2539–2549
55. Annamalai, B., Liu, X., Gopal, U., and Isaacs, J. S. (2009) Hsp90 is an essential regulator of EphA2 receptor stability and signaling: Implications for cancer cell migration and metastasis. *Mol. Cancer Res.* **7,** 1021–1032
56. Sreedhar, A. S., Soti, C., and Csermely, P. (2004) Inhibition of Hsp90: A new strategy for inhibiting protein kinases. *Biochim. Biophys. Acta* **1697,** 233–242
57. Songyang, Z. (1999) Recognition and regulation of primary-sequence motifs by signaling modular domains. *Prog. Biophys. Mol. Biol.* **71,** 359–372
58. Songyang, Z., Lu, K. P., Kwon, Y. T., Tsai, L. H., Filhol, O., Cochet, C., Brickey, D. A., Soderling, T. R., Bartleson, C., Graves, D. J., DeMaggio, A. J., Hoekstra, M. F., Blenis, J., Hunter, T., and Cantley, L. C. (1996) A structural basis for substrate specificities of protein Ser/Thr kinases: primary sequence preference of casein kinases I and II, NIMA, phosphorylase kinase, calmodulin-dependent kinase II, CDK5, and Erk1. *Mol. Cell. Biol.* **16,** 6486–6493
59. Modi, S., Stopeck, A., Linden, H., Solit, D., Chandarlapaty, S., Rosen, N., D'Andrea, G., Dickler, M., Moynahan, M. E., Sugarman, S., Ma, W., Patil, S., Norton, L., Hannah, A. L., and Hudis, C. (2011) HSP90 inhibition is effective in breast cancer: A phase II trial of tanespimycin (17-AAG) plus trastuzumab in patients with HER2-positive metastatic breast cancer progressing on trastuzumab. *Clin. Cancer Res.* **17,** 5132–5139
60. Pashtan, I., Tsutsumi, S., Wang, S., Xu, W., and Neckers, L. (2008) Targeting Hsp90 prevents escape of breast cancer cells from tyrosine kinase inhibition. *Cell Cycle* **7,** 2936–2941
61. Shimamura, T., Li, D., Ji, H., Haringsma, H. J., Liniker, E., Borgman, C. L., Lowell, A. M., Minami, Y., McNamara, K., Perera, S. A., Zaghlul, S., Thomas, R. K., Greulich, H., Kobayashi, S., Chirieac, L. R., Padera, R. F., Kubo, S., Takahashi, M., Tenen, D. G., Meyerson, M., Wong, K. K., and Shapiro, G. I. (2008) Hsp90 inhibition suppresses mutant EGFR-T790M signaling and overcomes kinase inhibitor resistance. *Cancer Res.* **68,** 5827–5838
62. Wright, T. M., Brannon, A. R., Gordan, J. D., Mikels, A. J., Mitchell, C., Chen, S., Espinosa, I., van de Rijn, M., Pruthi, R., Wallen, E., Edwards, L., Nusse, R., and Rathmell, W. K. (2009) Ror2, a developmentally regulated kinase, promotes tumor growth potential in renal cell carcinoma. *Oncogene* **28,** 2513–2523
63. Enomoto, M., Hayakawa, S., Itsukushima, S., Ren, D. Y., Matsuo, M., Tamada, K., Oneyama, C., Okada, M., Takumi, T., Nishita, M., and Minami, Y. (2009) Autonomous regulation of osteosarcoma cell invasiveness by Wnt5a/Ror2 signaling. *Oncogene* **28,** 3197–3208
64. Lara, E., Calvanese, V., Huidobro, C., Fernández, A. F., Moncada-Pazos, A., Obaya, A. J., Aguilera, O., González-Sancho, J. M., Sánchez, L., Astudillo, A., Muñoz, A., López-Otín, C., Esteller, M., and Fraga, M. F. (2010) Epigenetic repression of ROR2 has a Wnt-mediated, pro-tumourigenic role in colon cancer. *Mol. Cancer* **9,** 170
65. Nishita, M., Enomoto, M., Yamagata, K., and Minami, Y. (2010) Cell/tissue-tropic functions of Wnt5a signaling in normal and cancer cells. *Trends Cell Biol.* **20,** 346–354
66. Luque, A., Carpizo, D. R., and Iruela-Arispe, M. L. (2003) ADAMTS1/METH1 inhibits endothelial cell proliferation by direct binding and sequestration of VEGF165. *J. Biol. Chem.* **278,** 23656–23665
67. Gur, G., Rubin, C., Katz, M., Amit, I., Citri, A., Nilsson, J., Amariglio, N., Henriksson, R., Rechavi, G., Hedman, H., Wides, R., and Yarden, Y. (2004) LRIG1 restricts growth factor signaling by enhancing receptor ubiquitylation and degradation. *EMBO J.* **23,** 3270–3281
68. Laederich, M. B., Funes-Duran, M., Yen, L., Ingalla, E., Wu, X., Carraway, K. L., 3rd, and Sweeney, C. (2004) The leucine-rich repeat protein LRIG1 is a negative regulator of ErbB family receptor tyrosine kinases. *J. Biol. Chem.* **279,** 47050–47056
69. Segatto, O., Anastasi, S., and Alemà, S. (2011) Regulation of epidermal growth factor receptor signalling by inducible feedback inhibitors. *J. Cell Sci.* **124,** 1785–1793
70. Kao, Y. R., Shih, J. Y., Wen, W. C., Ko, Y. P., Chen, B. M., Chan, Y. L., Chu, Y. W., Yang, P. C., Wu, C. W., and Roffler, S. R. (2003) Tumor-associated antigen L6 and the invasion of human lung cancer cells. *Clin. Cancer Res.* **9,** 2807–2816